Ann. Geophys., 31, 197–208, 2013
www.ann-geophys.net/31/197/2013/
doi:10.5194/angeo-31-197-2013

Annales Geophysicae
Open Access

Simultaneous measurement of OI 557.7 nm, O_2 (0, 1) Atmospheric Band and OH (6, 2) Meinel Band nightglow at Kolhapur (17° N), India

N. Parihar[1], **A. Taori**[2], **S. Gurubaran**[3], **and G. K. Mukherjee**[4]

[1]Dr. K. S. Krishnan Geomagnetic Research Laboratory, Indian Institute of Geomagnetism, Allahabad 221 505, India
[2]National Atmospheric Research Laboratory, Gadanki 517 112, India
[3]Equatorial Geophysical Research Laboratory, Indian Institute of Geomagnetism, Tirunelveli 627 011, India
[4]Indian Institute of Geomagnetism, Navi Mumbai 410 218, India

Correspondence to: N. Parihar (navindeparihar@gmail.com)

Received: 9 October 2012 – Revised: 5 January 2013 – Accepted: 7 January 2013 – Published: 7 February 2013

Abstract. Near-simultaneous measurements of OI 557.7 nm, O_2 (0, 1) Atmospheric Band and OH (6, 2) Meinel Band nightglow were carried out at Kolhapur (17° N), India during February–March 2007. Atmospheric temperatures around 87 and 94 km were derived from the knowledge of intensity measurements of spectral features OH (6, 2) Meinel Band and O_2 Atmospheric Band, respectively. An account of the behaviour of derived temperatures has been presented. The nocturnal behaviour of OH and O_2 temperatures is governed by the waves of tidal origin, whereas the signatures of planetary wave-like oscillations is noted in the night-to-night variation of two temperatures. This is probably the first report of planetary waves observed in nightglow temperatures from the Indian subcontinent.

Keywords. Atmospheric composition and structure (airglow and aurora) – Meteorology and atmospheric dynamics (middle atmosphere dynamics: waves and tides)

1 Introduction

The mesosphere–lower thermosphere (MLT) is an important atmospheric region between 80 and 105 km characterized by unique thermal structure (negative temperature gradient in mesosphere, a pronounced minimum at mesopause and positive temperature gradient in thermosphere), complex chemistry, radiative cooling, dynamics and transport processes. Due to the photodissociative action of the incoming solar ultraviolet radiation (on O_2, O_3, H_2, H_2O and CH_4) in the MLT region and the associated transport processes, this region hosts several active chemical species primarily grouped into two families, viz. the O_x and HO_x families (Smith, 2004; Brasseur and Solomon, 2005). The species of these two chemical families participate in numerous exothermic reactions that strongly depend upon the local density of atomic oxygen. Some among them result in the formation of the excited products that cause the airglow phenomena. Consequently, nightglow is the characteristic feature of the MLT region.

The OH Meinel Band system, O_2 Atmospheric Band system and OI 557.7 nm emission are the prime atomic oxygen dependent emissions originating from the altitude of 87 km, 94 km and 97 km, respectively within the MLT region (Greer et al., 1986; Baker and Stair, 1988). The following reactions (known as *hydrogen-ozone reaction* and *Barth's excitation mechanism*) are the source of the excited OH molecules, O (^{1}S) atoms and O_2 ($b^1\Sigma_g^+$) molecules, respectively (see e.g. Bates and Nicolet, 1950; Bates, 1992, and references cited therein):

$$O_3 + H \rightarrow O_2 + OH^* \quad (1)$$

$$O + O + M(O_2 \quad \text{or } N_2) \rightarrow O_2^* + M \quad (2a)$$

$$O_2^* + O \rightarrow O_2 + O(^1S) \quad (2b)$$

$$O_2^* + O_2 \rightarrow O_2(b^1\Sigma_g^+) + O_2 \quad (2c)$$

Clearly, the excitation mechanisms involved suggest that the intensity of these emissions depends primarily on the local density of atomic oxygen which in turn is influenced by the perturbations due to gravity waves, tides and planetary waves. The propagation of gravity waves and atmospheric tides induces a change in the density of reacting species and the ambient temperature. The alterations produced in density as well as temperature in turn affect the rate of the airglow producing photochemical reaction, and these changes are reflected as variations in airglow intensity (Takahashi et al., 1979, 1998; Ward, 1998).

The ground-based observations of the nightglow phenomenon constitute one of the most widely used *remote sensing* techniques to explore the mesopause region, and recently, much attention is being paid to the aeronomy of the upper middle atmosphere using simultaneous measurements of the different nightglow emissions depending upon atomic oxygen (mainly OH Meinel Band, O_2 Atmospheric Band and the OI 557.7 nm emission as mentioned). Such studies provide valuable information regarding the chemistry and transport processes, dynamics and thermal structure of the MLT region. The advantage of using OH and O_2 Atmospheric Band airglow to study the MLT region is that the emission intensity and the atmospheric temperature around the emission peak can be measured simultaneously, and together with the measurement of the OI 557.7 nm emission such studies have great potential to understand the aeronomy of the MLT region. Previously, Hecht et al. (2004) deduced the atomic oxygen density from such simultaneous measurements, Takahashi et al. (1996) retrieved the night-time atomic hydrogen and ozone concentrations, Broadfoot and Gardner (2001) investigated the vertical transport of the mesospheric constituents, Molina et al. (1985) and Fagundes et al. (1995) studied the short-period quasi-coherent temporal variations (i.e. gravity wave phenomenology), Takahashi et al. (1998) investigated the influence of semidiurnal and diurnal tides on OH (9, 4) band, O_2 (0, 1) band and the OI 557.7 nm emission, and Buriti et al. (2005) studied the occurrence of planetary waves in the MLT region. Yee et al. (1997) made a quantitative comparison of near-simultaneous photometric observations of several OH Meinel Bands, O_2 (0, 1) Atmospheric Band and the OI 557.7 nm emission brightness and near-global measurements by the HRDI instrument onboard the UARS satellite, and also incorporated the mesospheric nightglow photochemistry into the 3-dimensional NCAR TIME-GCM model.

Motivated by these precedents, the simultaneous ground-based nightglow observations of the near-infrared OH (6, 2) Meinel Band, the O_2 (0, 1) Atmospheric Band and the OI 557.7 nm emission were carried out at a low-latitude station, Kolhapur (17° N), located in Peninsular India, during February–March 2007. The intensity of the spectral features of OH (6, 2) Meinel Band and O_2 (0, 1) Atmospheric Band nightglow has been utilized to derive the atmospheric temperatures near the corresponding emission peaks, viz. 87 and 94 km, respectively (Greer et al., 1986; Baker and Stair, 1988). Herein, an account of temperature measurements and dynamical features present in the data has been presented. Previously, Taori et al. (2012a, b, c) have reported the observations of OH and O_2 temperatures using mesosphere–lower thermosphere photometer (MLTP) measurements over Gadanki (13.5° N, 79.2° E), India. Using MLTP observations during April and July 2009, Taori et al. (2012a, c) presented the observations of gravity wave activity in OH and O_2 temperatures over Gadanki, whereas Taori et al. (2012b) found semiannual oscillations in two temperatures during April 2009–March 2011. The nocturnal behaviour of the intensity of OI 557.7 nm emission, noted in the present study, is quite similar to that reported earlier from the current observation site by Parihar et al. (2011), and hence, a brief report of observations of OI 557.7 nm emission during February–March 2007 has been presented here.

2 Derivation of OH and O_2 rotational temperatures

It is well known that OH/O_2 vibrational temperatures are very high, but rotational temperatures are thermalized and therefore correspond to the kinetic temperature of the local gas (see e.g. Sivjee and Hamwey, 1987, and references cited therin; Clemesha et al., 1990; Scheer and Reisin, 1990). Hence, OH and O_2 rotational temperatures can be assumed to represent the temperature around the mesopause heights of 87 (±4) and 94 (±3) km, respectively. The initial populations of the excited products (formed from the Eqs. 1 and 2c) are significantly non-thermal. However, due to the combined effect of the large radiative lifetime (∼50 ms for OH and ∼100 s for O_2) and the collision frequency prevailing at mesopause heights (∼10^4 s^{-1}, see e.g. US Standard Atmosphere, 1976), the excited OH and O_2 rotational population distribution quickly attains thermal equilibrium after being newly formed. For such a thermalized distribution, the photon intensity of a particular rotational line depends exponentially on the kinetic temperature (Mies, 1974). Thus, the intensity information of the thermalized distribution of the excited OH and O_2 molecules can be used to retrieve their kinetic temperature, and these spectroscopically determined temperatures are good proxy of atmospheric temperatures around 87 and 94 km altitude, respectively (see e.g. She and Lowe, 1998). Herein, the OH temperatures have been derived from the ratio of emission intensity of the P_1 (2) to P_1 (4) line of the OH (6, 2) Meinel Band (Parihar and Mukherjee, 2008), whereas the O_2 temperature was derived from the slope of the P branch spectrum integrated intensities (the P branch peak at 866 nm and the P branch at 868 nm) (Scheer, 1987). The estimated uncertainty in the derived OH and O_2 temperatures is 5 K and 6 K, respectively.

3 Instrumentation, results and discussion

Ground-based nightglow measurements of OH (6, 2) Meinel Band at 834.2 nm, O_2 (0, 1) Atmospheric Band at 864.5 nm and OI 557.7 nm were carried out at Kolhapur (16.8° N, 74.1° E), India. An all-sky scanning photometer (having a filter wheel assembly hosting six optical filters and a field of view of 7.25°) was deployed for simultaneous monitoring of different emission features on clear sky conditions and moonless nights centred on the new moon period during February–March 2007. For simplicity, this photometer was operated for observations in the zenith only. An RCA 31034A (GaAs photocathode) photomultiplier (thermoelectrically cooled at −25 °C) was utilized for photon detection. The P_1 (2) −839.9 nm and P_1 (4) −846.6 nm lines of OH (6, 2) Meinel Band, O_2 (0, 1) Atmospheric Band P branch spectrum (one at 866 nm and another at 868 nm) and the OI 557.7 nm emission were monitored using filters of half-power bandwidth ∼0.80 nm. The background emission at 857 nm filter ($\Delta\lambda \sim 1.20$ nm) was also measured. All optical filters were maintained at 25 °C. Each emission feature was observed for 120 s with a delay of 30 s (i.e. the integration and delay time for each filter were so adjusted to have a scan interval of 15 min). The corrections for the transparency of filters, photomultiplier dark current and sensitivity of the photomultiplier tube with respect to a particular wavelength were carried out. Hopefully, the intensity measurements will be presented in absolute Rayleigh units in near future. Due to good weather conditions prevailing during February–March 2007, the continuous night-to-night monitoring of nightglow features for more than 9 days during each month was possible. In this paper, the useful data of 21 nights (11 nights of February and 10 nights of March) having observation periods of more than 6 h have been presented. On most of the nights, the duration of continuous monitoring of the nightglow features was ∼8.5 h.

3.1 Observed OH and O_2 temperatures

Figure 1 summarizes the nocturnal mean values of the derived O_2 and OH temperatures during February–March 2007. The O_2 and OH temperatures are represented by the solid and open circles, respectively. Also shown in the plot is the standard error of the mean (represented by error bars) of the two temperatures during the night. To avoid overlap of error bars, OH measurements have been shown slightly displaced along the x-axis with respect to O_2. The nightly mean O_2 temperature varies from 187 K to 198 K, whereas the OH ones lies between 190 K and 204 K. It can be seen that the nightly mean temperatures vary in a narrow temperature band of 17 K, and the deviation of either temperature is 7 K or less for most of the nights. Also, the OH temperatures were warmer (on an average by 5 K) than the O_2 ones. Scheer and Reisin (1990), Takahashi et al. (1986) and Gavrilyeva and Ammosov (2004) have reported similar observations. During February, the nocturnal mean O_2 temperatures mostly lay in a band of 2 K centred on 193 K, whereas the variation of OH ones were larger. And it suggests that the O_2 layer was more stable than the OH layer with respect to temperature perturbations. Scheer and Reisin (1990) have also reported similar observations and described it as the appearance of a "quiet layer" in the neighbourhood of strong oscillations. On 13–14 March 2007, the mean OH temperature was about 1 K greater than the O_2 temperature. An account of the nocturnal variation of the two temperatures on this particular night is presented below. The average O_2 and OH temperature observed during the entire campaign period was 192.2 ± 5.3 K and 197.4 ± 6.3 K, respectively. On most nights, the standard error of mean for O_2 and OH temperatures was 0.8 K and 1.0 K, respectively, and overall the standard error was less than 1.3 K. Similar mean values have been reported previously for low-latitude sites in India; see Table 1. At Pune (18° N, 73° E), India, Agashe et al. (1989) found the OH temperatures of 195 ± 10 K. Sridharan et al. (1999) reported the measurements of daytime OH temperatures (∼185 K) over Tirunelveli (8.7° N, 77.8° E), India. Parihar and Mukherjee (2008) observed the mean OH temperature of 195 K during November 2002–May 2005 from the present site. A comparison with the MSISE-90 model indicates that the model predictions are 5–7 K lower than the observed temperatures. Figure 2 depicts the frequency of occurrence of the O_2 and OH temperatures (shown by solid and open circles, respectively) at intervals of 5 K. The total number of observations for the entire database of the individual temperatures was 749. The solid curves in the plots represent the respective Gaussian fit to the observed frequency. A good correspondence between the applied fit and the observed frequency can clearly be seen in both plots. It indicates that the normal temperature at 87 K and 94 km is 196 K and 191 K, respectively, and these values are very close to the mean OH and

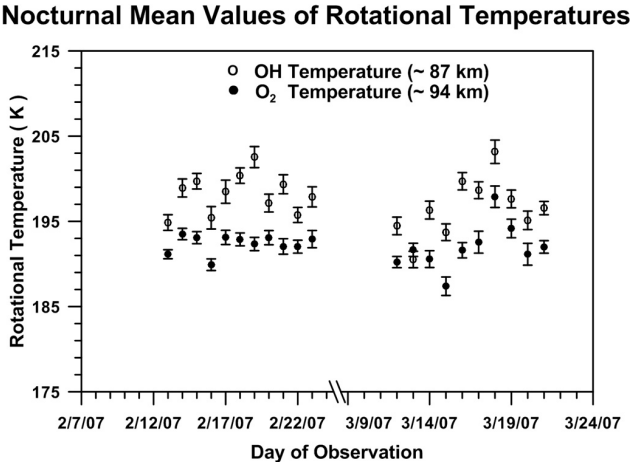

Fig. 1. Nocturnal mean values of OH and O_2 temperatures at Kolhapur during February–March 2007.

Table 1. Mean temperatures observed in India using the ground-based measurements of OH Meinel Band airglow.

Observing site in India	Mean temperature	Reference
Pune (18° N, 73° E)	195 ± 10 K	Agashe et al. (1989)
Tirunelveli (8.7° N, 77.8° E)	∼185 K	Sridharan et al. (1999)
Kolhapur (16.8° N, 74.1° E)	195 K	Parihar and Mukherjee (2008)

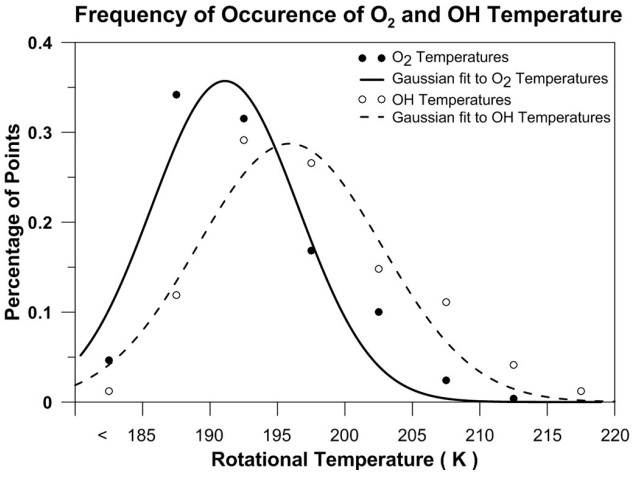

Fig. 2. Frequency of occurrence to O_2 and OH temperatures at Kolhapur during February–March 2007.

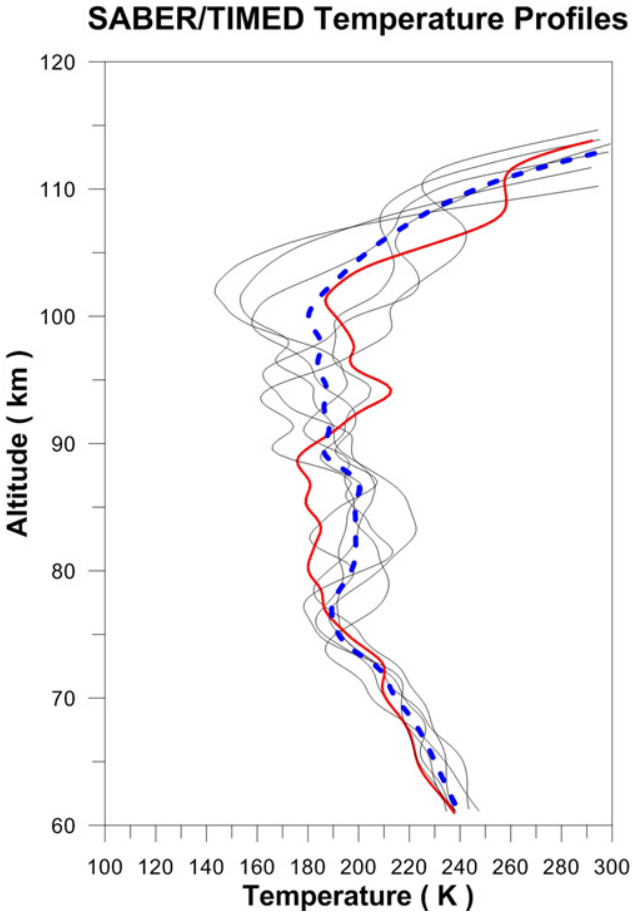

Fig. 3. Temperature profiles of SABER/TIMED overpasses for 12°–22° N latitude and 69°–79° E longitude range during February–March 2007.

O_2 temperatures, viz. 197.4 K and 192.2 K, respectively. It is worth mentioning that the standard error of mean temperature is ∼1 K. About 66 % of O_2 temperature measurements lie in the range of 186–196 K, whereas for OH measurements 55 % of points are subsumed between 191 K and 201 K.

As the temperature information of two different altitudes was available, an attempt to infer the temperature gradient persistent in the MLT region was made. Such a gradient should provide an important insight of the mesospheric thermal structures. Assuming that the altitude of the emission peak of OH Meinel Band and O_2 Atmospheric Band is located at 87 km and 94 km, respectively (Greer et al., 1986; Baker and Stair, 1988) and remained unchanged during the course of the night, the temperature gradient near the mesopause region was calculated from the two temperature datasets and an average negative temperature gradient of 0.8 K per km was found, which suggests a mesopause height close to or higher than the O_2 emission height. Using the temperature profiles measurements by the SABER instrument on-board TIMED satellite, Xu et al. (2007) found the altitude of mesopause to be around 98 km during February–March for near Kolhapur locations. Figure 3 shows the SABER/TIMED temperature profiles for 12°–22° N latitude and 69°–79° E longitude range on coincidental nights during February–March 2007. The continuous curves depict the temperature profiles measured by the SABER instrument, while the averaged temperature profile for entire observation period is shown by the dashed curve. Although the SABER profiles are highly perturbed, it is quite clear that mesopause is located above 90 km (the temperatures are comparatively higher near the assumed OH emission peak of 87 km than the O_2 one at 94 km). An average negative temperature gradient of 1.6 K per km was also noted between 87 km and 94 km in the SABER measurements.

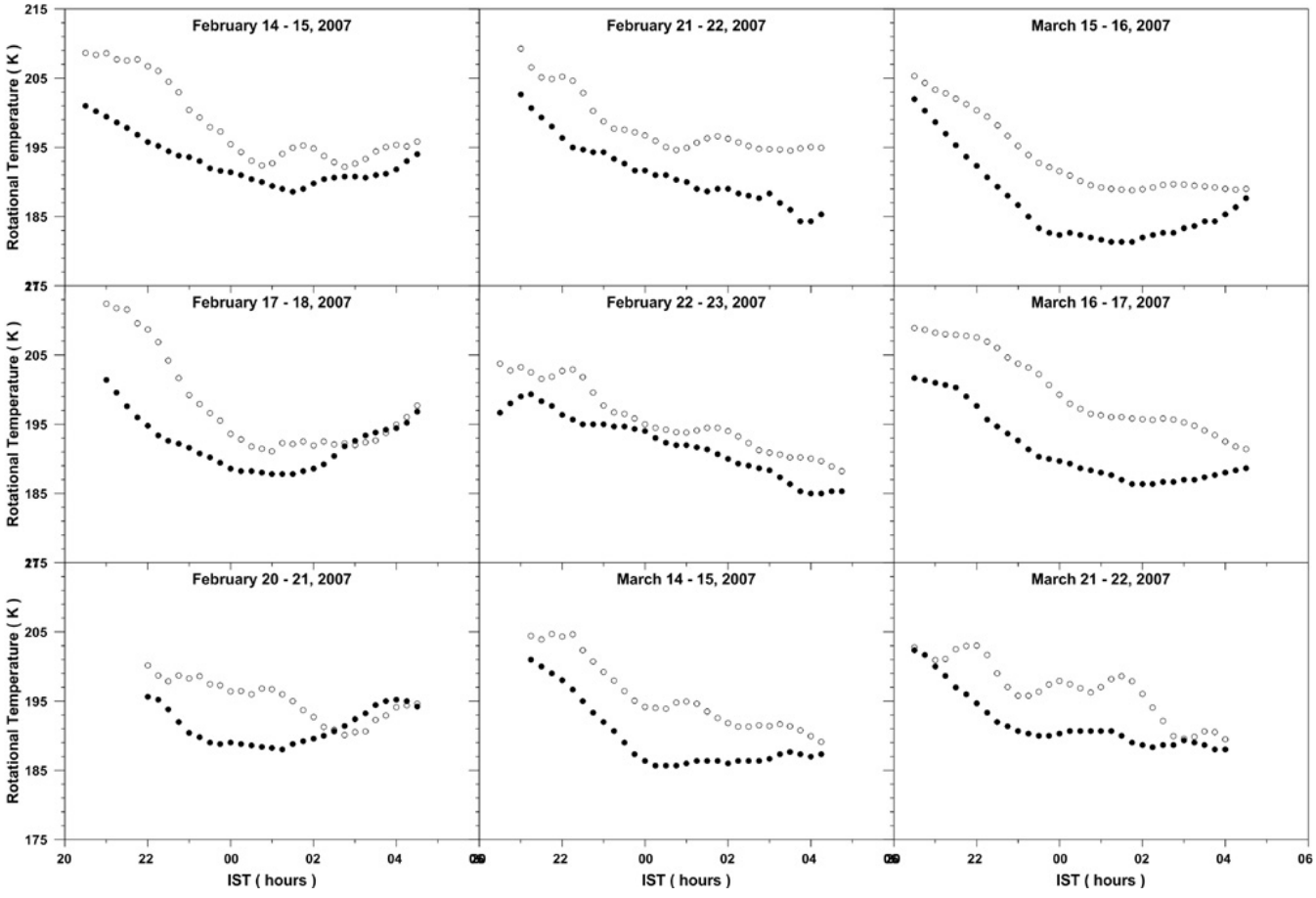

Fig. 4. Nocturnal variation of OH (open circles) and O_2 (solid circles) temperatures during some nights.

3.2 Nocturnal behaviour of OH and O_2 temperatures and observations of tide-like long-period oscillations

Figure 4 presents some typical examples of the nocturnal variations of the derived rotational temperature OH (open circles) and O_2 (solid circles) temperatures. Each nightly temperature dataset on average consisted of 35 measurements. In order to bring out the long-period oscillation present in the temperature datasets, the five-point running means have been presented in the plot with the same temperature and time scales to facilitate direct comparison. It can be seen that both temperatures decrease from late dusk hours to midnight hours, and this was the general situation for all 21 nights. On most occasions a post-midnight increase in the two temperature series was observed, and the lowest temperatures occurred generally around 00:15–02:15 IST. The plots for 14–15, 17–18, 20–21 February, and 15–16 March 2007 represent examples of this observed variation. Such a feature of the pre-midnight decrease, a minimum around local midnight and a post-midnight increase has been attributed to the temperature and density variation produced by tides in the course of their propagation through the emission layer (Petitdidier and Teitelbaum, 1977; Takahashi et al., 1998; Zhang and Shepherd, 1999). Atmospheric tides are global scale oscillations created in the lower and middle atmosphere due to absorption of solar infrared and ultraviolet radiation by the tropospheric water vapour and stratospheric ozone, respectively, and have frequencies that are an integral fraction of the diurnal oscillation. A similarity in the shape of variation of two temperature series can be seen, and such similarity suggests that the response of the two emission layers is same with respect to the longer period dynamical perturbation. However, a discrepancy exists in the two temperature series with respect to the short-period oscillations – the oscillatory features present in the OH temperature series were not present in the O_2 temperature series. Most likely, the waves observed in OH temperature series (probably due to gravity wave activity) dissipated below O_2 emission peak on the course of their propagation. The plot for 21–22 March 2007 in Fig. 4 depicts an example of such a feature – the variation of O_2 temperature is fairly steady, whereas the one of OH is marked by oscillations having periodicity of $\sim$2 h. From an analysis for the short period variations in the OH temperature series, the oscillations having periodicities in the range of 1–2 h dominate the spectrum of gravity wave activity near the OH

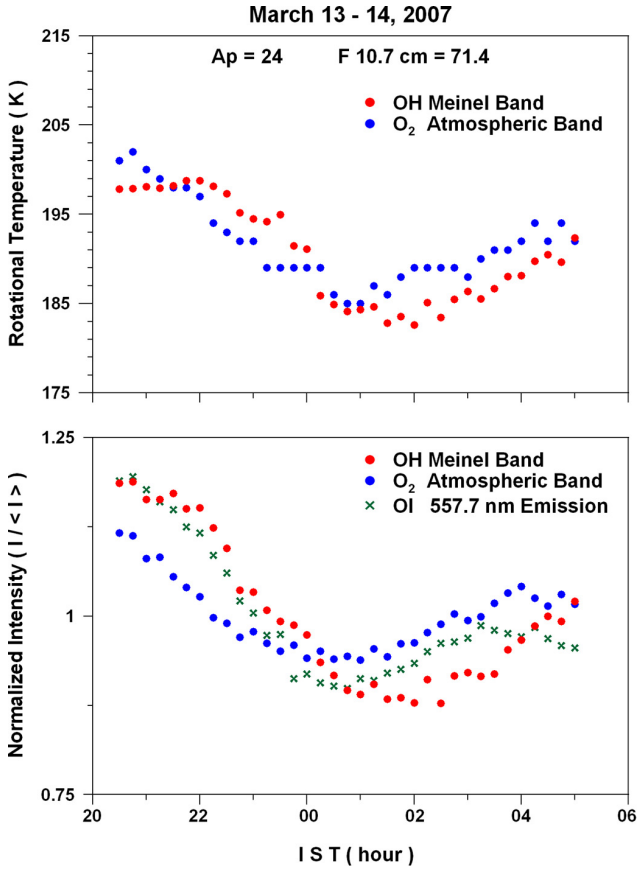

Fig. 5. Nocturnal variations of the emission intensities and derived temperature observed on 13–14 March 2007.

emission peak. Parihar et al. (2011) had similar observations for concurrent database of OH temperature and OI 557.7 nm emission intensity (i.e. the short-period oscillations observed in OH temperature series were not seen in OI 557.7 nm intensity data) on most occasions. On rest of the nights, the temperature variation was marked by a monotonous decrease from beginning of the night to dawn hours. In Fig. 4, the variations observed on 22–23 February 2007 portray an example of such a monotonic decrease.

Also, the trends of the intensity and corresponding temperature variation closely resemble each other for both OH and O_2 measurements (i.e. the characteristic shape of the two intensity series were complimented often by a concurrent feature in the variations of corresponding temperatures). Figure 5 presents an example of such correlated variation of the different observed quantities. The bottom panel shows the observed variation of OH (open circle) and O_2 (solid circles) emission intensities along with the OI 557.7 nm emission (crosses), and the top panel depicts the variation of the derived OH (open circle) and O_2 (solid circles) temperatures. For simplicity, the normalized values of intensities have been presented. On the whole, OH and O_2 temperature variations co-vary during the nights. A cross-correlation analysis of different quantities for entire database indicates that in general, OI 557.7 nm intensity variations lead that of O_2 measurements by 15–30 min, whereas O_2 intensity and temperature measurements lead the OH ones by 45–60 min. Such correlated behaviour of OI 557.7 nm, O_2 Atmospheric Band and OH Meinel Band nightglow has been attributed to the dependence of their excitation mechanism on the local density of atomic oxygen that in turn is controlled by the transport and recombination processes prevailing in the MLT region (Brasseur and Solomon, 2005).

On one particular night, 13–14 March 2007 (shown in Fig. 5), the mean temperature at OH altitude (∼87 km) was greater than the O_2 temperature. The SABER/TIMED temperature profile for this particular night (shown by red curve in Fig. 3) indicates a strong temperature inversion of about ∼23 K at around 93–94 km. At 87 km and 94 km, the temperatures were ∼180 K and 213 K, respectively. In post-midnight hours, the O_2 intensity, OI 557.7 nm intensity and O_2 temperature increase at a higher rate compared to those of OH measurements. It can be interpreted as a direct consequence of strong temperature inversion around 94 km. Taori et al. (2012c) have reported such variability of OH and O_2 temperature over Gadanki (13.5° N, 79.2° E), India due to convective activity during April 2009.

Together, Figs. 4 and 5 indicate that the long-period tide-like oscillations dominate the temperature variations. On such nights, the minima of intensity generally occurred around midnight (between 00:00 and 02:00 IST). As the length of time series discussed herein was limited to ∼8.5 h, the exact determination of periodicity of the long-period waves apparent in data was not possible. However, an attempt to identify the tidal feature present in dataset has been made using the sinusoidal least square fitting method. In such analysis, a sinusoidal least square fit of form $[A\mathrm{Sin}(2\pi t/T+\varphi)+c]$ was forced on the time series of observed features (viz. OI 557.7 nm intensity, O_2 intensity and temperature, OH intensity and temperature) with the wave period, T, as 8 h, 12 h and 24 h for a particular night and then root mean square error was estimated for each value of T (here, A is the amplitude of wave, T is the wave period, φ represents the phase of the wave, and c is the constant term). Such analysis indicates that a 12-h wave fitting explains the nocturnal behaviour of observed features in a better way in comparison to the 8-h and 24-h fits in most cases.

Alternatively, the Lomb–Scargle periodogram analysis of the dataset of individual features was performed. Results of this analysis are tabulated in Table 2 (the values in braces represent the individual contribution). It can clearly be noted that the 12-h component is the primary one and appears to be a consistent tidal feature (with a contribution of about 41 %) during each month. During February, the semidiurnal contribution was fairly stronger than that of the diurnal component at 97 km altitude; however, around 87 km, the contributions from the two harmonics were quite comparable. Hence, it is assumed that the long-period oscillations

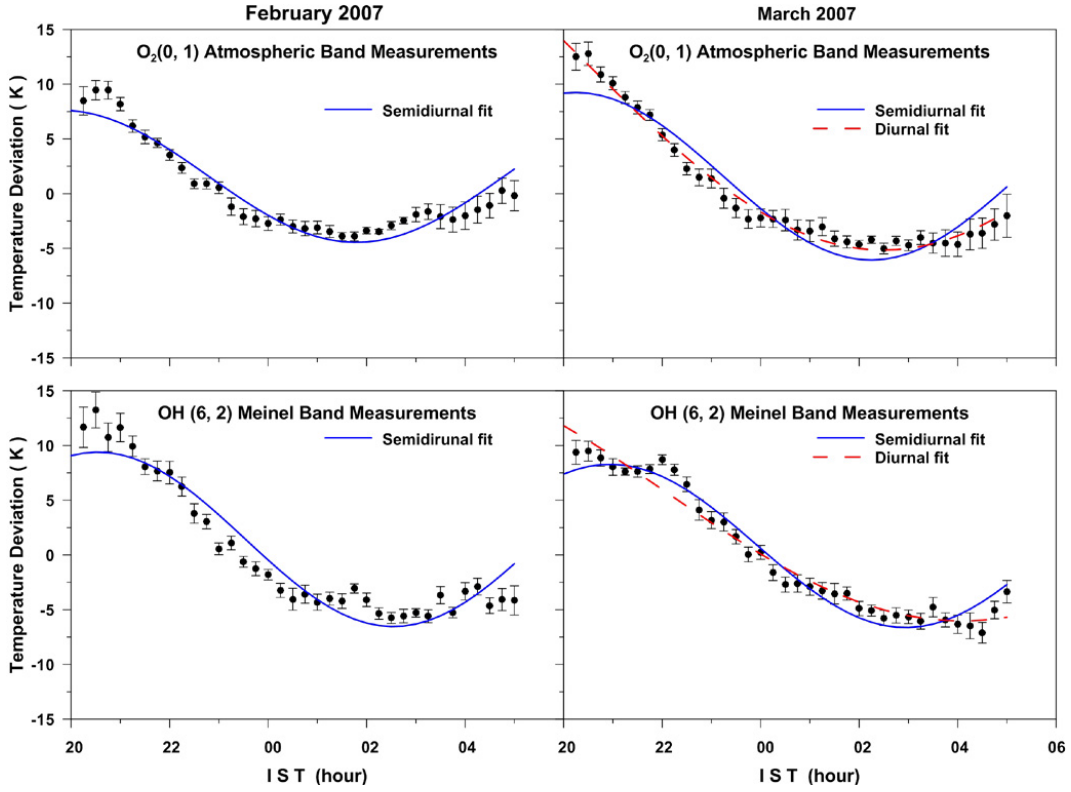

Fig. 6. Averaged nocturnal variation of OH and O_2 temperature for February and March 2007 along with the forced tidal fit based on Lomb–Scargle analysis.

in the observed quantities are driven by (i) a semidiurnal tide during February and (ii) an equivalent mixture of diurnal and semidiurnal tides during March. Now, the issue was to have an estimate of the amplitude and phase of the tidal waves observed in the temperature dataset. For this, (i) the nocturnal mean value was subtracted from the time series of temperature for a night, (ii) the averaging of temperature at each timestamp for a particular month was carried out, and (iii) the sinusoidal least square fit was applied to the averaged time series with periods of 12 h and 24 h (based on Lomb–Scargle analysis for an individual month). It is worth mentioning here that the night-to-night variation of phase of forced fit (either 12-h or 24-h fit) of individual nights was less than an hour, and following this, it is assumed that the tidal information was retained in the averaging process. Figure 6 presents the monthly mean nocturnal variation of OH and O_2 temperature (along with the respective standard error of means as error bars) for February and March 2007 (left and right panel, respectively). The solid curves represent the semidiurnal fit to the data, whereas the diurnal fits are shown as broken curves. A close correspondence between the observed variations and forced harmonic fit can clearly be seen at all altitudes. Clearly (as expected from Table 2), the temperature variations during February are governed by a semidiurnal tide. In February, the quality of semidiurnal fit appears comparatively better at O_2 heights than OH ones. During March, the quality of semidiurnal and diurnal fits appears similar at OH heights, but at O_2 altitude, diurnal fit looks a bit better. We compute the phase velocity of wave and vertical wavelength using the phase information of the forced tidal feature at different altitudes. Table 3 summarizes the characteristics of semidiurnal and diurnal waves observed in the temperature dataset obtained from such analysis. During February–March, the inferred semidiurnal tidal amplitudes and phases lay in the range of 6–8 K and 4.5–5.5 h, respectively, and the vertical phase velocity was ∼9.6 km per h. For the diurnal tide observed during March, (i) the amplitude and phase at 87 km was 11.7 K and 10 h, respectively; (ii) at 94 km, the amplitude and phase was 16.9 K and 8.4 h, respectively, and (iii) the vertical phase velocity was 4.4 km per h. The vertical wavelengths of the observed tidal features were ∼110 km (significantly higher than typical value of ∼40–50 km per h). Similar tidal amplitudes have been reported in the literature. Using WINDII instrument (on board UARS satellite) and K-lidar temperature data, Shepherd and Fricke-Begemann (2004) found the semidiurnal tidal amplitudes at 89 km to lie in the range 2.2–8.8 K at 28° N and 55° N during November, December, January and February. The temperature measurements by the SABER instrument on board the TIMED satellite

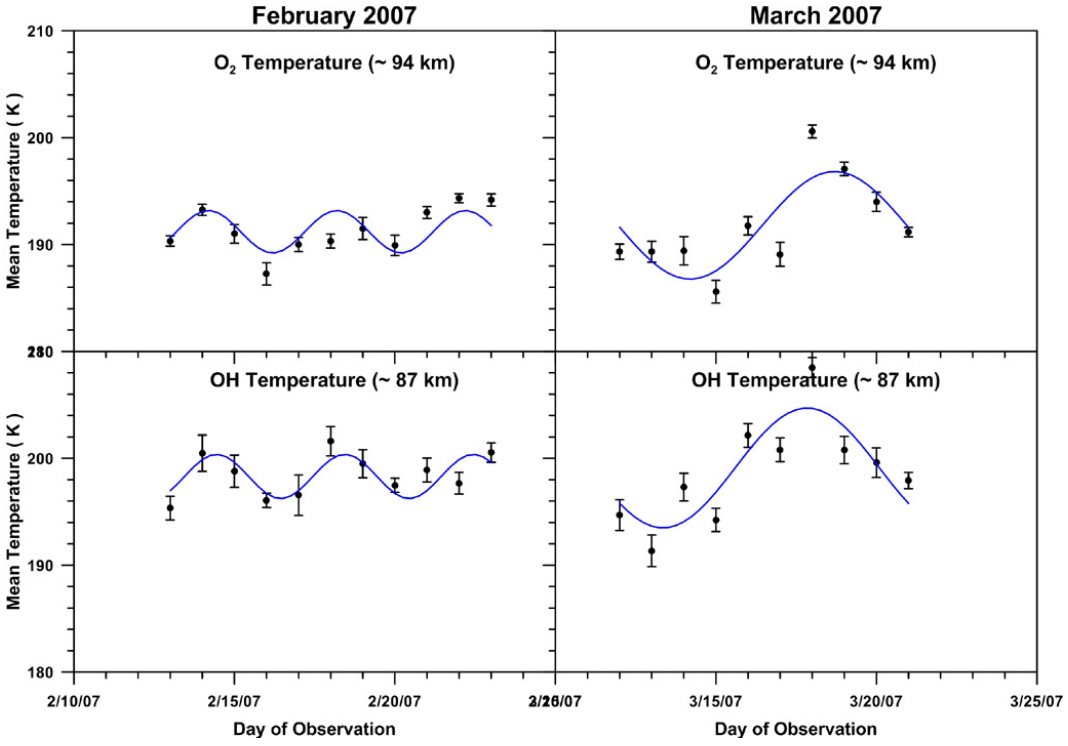

Fig. 7. Night-to-night variability of the averaged temperature between 22:00 h and 01:00 h at OH and O_2 altitudes during February and March 2007 along with the forced planetary wave fit based on Lomb–Scargle periodogram analysis.

have provided a unique global understanding of atmospheric tides. Zhang et al. (2006) noted migrating semidiurnal amplitudes of order of 4–6 K at 90 km for a latitude band of 0°–20° during February and March. In ±50° latitude range, Forbes et al. (2008) found the typical amplitudes of semidiurnal and diurnal tides in the range of 6–14 K and 8–18 K, respectively, in the MLT region during 2002–2006. Pancheva et al. (2009a) indicate the strongest migrating semidiurnal feature with amplitudes reaching ∼6 K around ±20–30° tropical latitudes at 90 km heights during 2002–2007. Around 90 km and in 15–18° latitude range, the Global Scale Wave Model (GSWM-00, http://www.hao.ucar.edu/modeling/gswm/gswm.html) estimates (i) semidiurnal tidal amplitudes in 0.7–1.9 K range and phase to vary from 6–16 h during February–March, and (ii) diurnal tidal amplitudes ∼5 K and phases ∼19 h.

3.3 Signatures of planetary wave-like oscillations in OH and O_2 temperatures

As continuous night-to-night dataset for more than 9 days during each month was available and the night-to-night tidal variability was not strong, an attempt to study the signatures of planetary wave activity has been made. In order to suppress the tidal contamination in planetary wave analysis, the average value of temperatures between 22:00 and 01:00 IST has been considered. It was observed during the tidal analysis that (i) the variation of tidal amplitude and phase from night-to-night was less than 1.2 K and 0.9 h, respectively during individual months, and (ii) the crest and trough of the tidal oscillations appear around 21:00 and 02:00 IST. Hence, the time interval of 22:00–01:00 IST was preferred. Figure 7 presents the night-to-night variability of this averaged temperature at OH and O_2 altitudes (bottom and top row, respectively) for each month. Herein, the error bar represents the standard error of the mean temperature during 22:00–01:00 IST. Lomb–Scargle analysis shows the same principal spectral component to be present at both OH and O_2 altitudes, viz. a 4-day wave during February and a 9-day wave during March. Similar analysis carried out using the difference of nightly mean temperature and its monthly mean value indicates a 3–4.5 and 9 day wave during February and March, respectively. Using periods obtained from Lomb–Scargle analysis, the sinusoidal least square fit was applied to the averaged temperature dataset and is shown by solid curves in Fig. 7. A good correspondence between the mean values and forced fit can clearly be seen at both altitudes, especially during February. The amplitude of observed 4-day and 9-day waves was 2 K and 5.3 K, respectively. Periods like those found at Kolhapur during February have been reported earlier at other low-latitude sites. Using MF radar wind measurements, Sridharan et al. (2002) reported observations of 3.5-day ultra fast Kelvin wave in the MLT region over Tirunelveli (8.7° N, 77.8° E), India. Takahashi et

Table 2. Monthly mean tidal components for each campaign at Kolhapur during February–March 2007 obtained by Lomb–Scargle periodogram analysis.

Month 2007	Harmonics present in the observed nightglow features (with descending contribution)			
	OI 557.7 nm intensity	O_2 intensity	O_2 temperature	OH intensity	OH temperature
February	12 h (0.43), 8 h (0.41), 24 h (0.16)	12 h (0.43), 8 h (0.32), 24 h (0.25)	12 h (0.43), 8 h (0.31), 24 h (0.26)	12 h (0.40), 24 h (0.38), 8 h (0.22)	12 h (0.41), 24 h (0.35), 8 h (0.24)
March	12 h (0.41), 8 h (0.31), 24 h (0.28)	12 h (0.42), 24 h (0.32), 8 h (0.26)	12 h (0.42), 24 h (0.34), 8 h (0.24)	12 h (0.40), 24 h (0.38), 8 h (0.22)	12 h (0.40), 24 h (0.37), 8 h (0.23)

al. (2002) observed 3.5-day planetary waves in OH, O_2 and OI 557.7 nm emissions over São João do Cariri (7° S, 37° W), Brazil. Over the same site, Buriti et al. (2005) observed an oscillation of 3–4 days in OI 557.7 nm, O_2 and OH emission intensities and OH temperature. Using the meteor radar wind measurements, Pancheva et al. (2004) reported strong 3–4 day oscillation in the zonal wind at Ascension Island (7.9° S, 14.4° W). Analyzing the SABER/TIMED temperature database in the latitudinal range 50° N–50° S, Pancheva et al. (2009b) found the dominance of four planetary wave features in the MLT region, viz. 24, 15–17, 10–12 and 5–6 days. Taori and Taylor (2010) reported the observations of quasi-5-day wave (having amplitude ∼8.5 K) in O_2 temperatures of the Mesospheric Temperature Mapper (MTM) database over Maui, Hawaii (20.8° N, 156.2° W). The 9-day wave observed during March is an interesting feature and has been reported in literature often. Mukhtarov et al. (2010) found prominent 9-day oscillation in the SABER/TIMED temperatures during 2005–2006 over the Arctic and associated it with the coronal hole feature of sun. Probably, this is the first report of planetary wave signatures in the nightglow temperature from the Indian subcontinent.

3.4 Observations of OI 557.7 nm emission

Figure 8 presents the nocturnal variation of intensity of OI 557.7 nm emission on some nights. As the intensities were not calibrated (due to unavailability of standard source of light), the variation of intensity normalized with respect to the mean value has been presented. A monotonous decrease of intensity from the beginning of night to midnight hours can be seen on most of the nights. Often, this decrease of intensity continued up to dawn hours and the variations observed on 22–23 February 2007 and 18–19 March 2007 are examples of such monotonic decrease. Such nocturnal behaviour of intensity of the atomic oxygen dependent nightglows from the MLT region has been attributed to the depletion of local density of atomic oxygen in absence of photolysis during the night. Sometimes the intensity remained reasonably steady after midnight hours (e.g. 21–22 February 2007). In most cases, an increase in intensity after midnight hours was seen, and often it continued beyond dawn hours. Most of the plots shown in Fig. 8 depict such behaviour of OI 557.7 nm emission at Kolhapur. On such nights, the minimum of intensity occurred between 00:00 h and 02:00 h. Such an observed feature has been explained in terms of an increase in atomic oxygen density induced by tidal oscillations in post-midnight hours (Takahashi et al., 1998). Ward (1998) modelled the local time variations of O (^{1}S) airglow induced by diurnal tides and found the changes in the atomic oxygen mixing ratio (due to vertical motions associated with tides) as the cause of such observed airglow variations. The visual inspection of plots shown in Fig. 8 does indicate the presence of tide-like oscillations. Lomb–Scargle analysis (presented in Table 2) suggests that the nocturnal

Table 3. Characteristics of semidiurnal and diurnal tidal features inferred using the sinusoidal least square fitting method.

Month 2007	Tidal feature observed	Amplitude		Vertical phase velocity	Vertical wavelength
		At 87 km	At 94 km		
February	Semidiurnal	7.9 K	6.1 K	9.3 km h^{-1}	112 km
March	Semidiurnal	7.5 K	7.7 K	10 km h^{-1}	120 km
	Diurnal	11.7 K	16.9 K	4.4 km h^{-1}	105 km

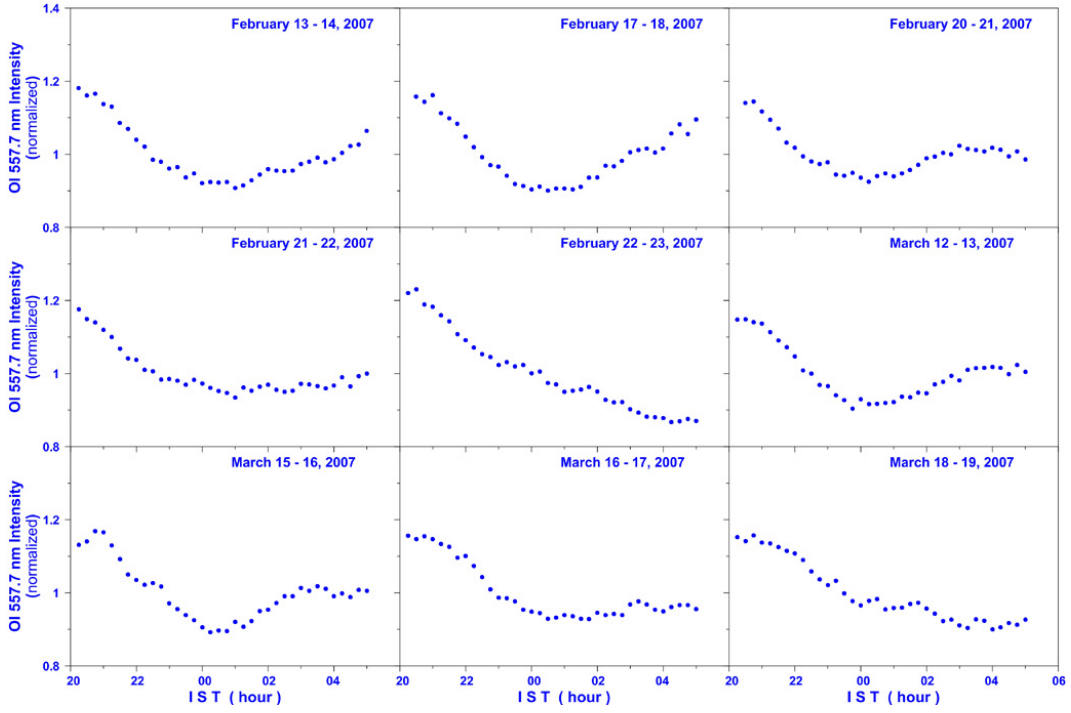

Fig. 8. Nocturnal variation of OI 557.7 nm emission intensity on some nights during February–March 2007 at Kolhapur.

behaviour of OI 557.7 nm emission intensity was governed by a semidiurnal tide during February–March. As done for the two temperatures, the sinusoidal least square fit analysis was performed, and the phase of semidiurnal tide came out to be 4.4 h and 4.8 h during February and March, respectively. Using the phase information of OI 557.7 nm emission and OH (6, 2) Meinel Band intensity measurements, the vertical phase velocity of 8.4 km per h and 9.1 km per h was estimated for semidiurnal tide during February and March, respectively. These values are close to those inferred from the temperature measurements. Unlike OH and O_2 temperature measurements, terdiurnal wave period was the second spectral component in OI 557.7 nm measurements.

4 Conclusions

Simultaneous observations of three different nightglow features from the MLT region ∼OH (6, 2) Meinel Band, O_2 (0, 1) Atmospheric Band and OI 557.7 nm emission have been carried out at Kolhapur, a low-latitude station in India, to study the dynamical features having timescales of half a day or more. Nightglow temperatures were inferred from OH and O_2 intensities (a proxy of atmospheric temperatures around 87 km and 94 km, respectively). The average OH and O_2 temperature was 197 K and 192 K, respectively. Also, the individual nocturnal mean temperatures were nearly always smaller for O_2 measurements than for OH, which suggests the mesopause to be located above or near O_2 emission altitude. The SABER/TIMED temperature profiles during the campaign period show similar feature. Nocturnal behaviour of two temperatures is governed by a semidiurnal tide during February, whereas a mixture of diurnal and semidiurnal tide explains the observed temperature variations during March. The night-to-night variability of two temperatures shows the presence of planetary wave features. The Lomb–Scargle analysis of temperature dataset suggests a 3–4.5- and 9-day wave during February and March, respectively. The

observed periods during February have been reported earlier by Sridharan et al. (2002) and Pancheva et al. (2009b). The nocturnal behaviour of OI 557.7 nm emission intensity is generally marked by a decrease from beginning of the night to midnight hours, followed by a minimum around 00:00–02:00 IST and an increase in post-midnight hours till dawn hours. Lomb–Scargle analysis suggests a semidiurnal tide to govern the variations of OI 557.7 nm emission intensity.

At present, Nainital (29.40° N, 79.50° E) and Gadanki (13.50° N, 79.20° E) are the two measurement sites from India forming part of the Network for the Detection of Mesopause Change (NDMC, http://wdc.dlr.de/ndmc/index.php). The efforts are on to carry out nightglow observations regularly (centred on new moon period) from another station at 23° N to continue airglow-based temperature studies in North India. In future, an extensive temperature database along with the complementary wind data will be taken up for a comprehensive study of tides and planetary waves, and the validation of observed rotational temperatures with the SABER/TIMED measurements will be done.

Acknowledgements. Nightglow measurements have been carried out at Kolhapur, India under scientific collaboration between Indian Institute of Geomagnetism, Navi Mumbai and Shivaji University, Kolhapur. The funds for the research studies are being provided by Department of Science and Technology (DST), Govt. of India, New Delhi. NP is thankful to Juergen Scheer (Instituto de Astronomia y Fisica del Espacio, Argentina) and Hisao Takahashi (Instituto Nacional de Pesquisas Espaciais, Brazil) for many fruitful communications and supplying relevant data, respectively. NP is grateful to both the referees for their esteemed comments in improving the manuscript.

Topical Editor C. Jacobi thanks P. Muralikrishna and one anonymous referee for their help in evaluating this paper.

References

Agashe, V. V., Pawar, V. R., Aher, G. R., Nighut, D. N., and Jehangir, A.: Study of mesopause temperature and its behavior from OH nightglow, Ind. J. Radio and Space Phys., 18, 309–314, 1989.

Baker, D. J. and Stair, A. T.: Rocket measurements of the altitude distributions of the hydroxyl airglow, Physica Scripta, 37, 611–622, 1988.

Bates, D. R.: Nightglow emissions from oxygen in the lower thermosphere, Planet. Space Sci., 40, 211–221, 1992.

Bates, D. R. and Nicolet, M.: The Photochemistry of Atmospheric Water Vapor, J. Geophys. Res., 55, 301–327, 1950.

Brasseur, G. and Solomon, S.: Aeronomy of the Middle Atmosphere: Chemistry and Physics of the Stratosphere and Mesosphere, Springer, The Netherlands, 2005.

Broadfoot, A. L. and Gardner, J. A.: Hyperspectral imaging of the night airglow layer from the shuttle: A study of temporal variability, J. Geophys. Res., 106, 24795–24812, 2001.

Buriti, R. A., Takahashi, H., Lima, L. M., and Medeiros, A. F.: Equatorial planetary waves in the mesosphere observed by airglow periodic oscillations, Adv. Space Res., 35, 2031–2036, 2005.

Clemesha, B. R., Takahashi, H., and Batista, P. P.: Mesopause temperatures at 23° S, J. Geophys. Res., 95, 7677–7681, 1990.

Fagundes, P. R., Takahashi, H., Sahai, Y., and Gobbi, D.: Observations of gravity waves from multispectral mesospheric nightglow emissions observed at 23° S, J. Atmos. Terr. Phys., 57, 395–405, 1995.

Forbes, J. M., Zhang, X., Palo, S., Russell, J., Mertens, C. J., and Mlynczak, M.: Tidal variability in the ionospheric dynamo region, J. Geophys. Res., 113, A02310, doi:10.1029/2007JA012737, 2008.

Gavrilyeva, G. A. and Ammosov, P. P.: Measurements of upper mesosphere temperature on the height of night sky emission excitation OH and O_2 (0-1) in Yakutsk in: Tenth Joint International Symposium on Atmospheric and Ocean Optics/Atmospheric Physics, Proceedings of the SPIE, 5397, 331–339, 2004.

Greer, R. G. H., Murtagh, D. P., McDade, I. C., Dickinson, P. H. G., Thomas, L., Jenkins, D. B., Stegman, J., Llewellyn, E. J., Witt, G., MacKinnon, D. J., and Williams, E. R.: Eton 1: A data base pertinent to the study of energy transfer in the oxygen nightglow, Planet. Space Sci., 34, 771–788, 1986.

Hecht, J. H., Liu, A. Z., Walterscheid, R. L., Roble, R. G., Larsen, M. F., and Clemmons, J. H.: Airglow emissions and oxygen mixing ratios from the photometer experiment on the Turbulent Oxygen Mixing Experiment (TOMEX), J. Geophys. Res., 109, D02S05, doi:10.1029/2002JD003035, 2004.

Mies, F. H.: Calculated vibrational transition probabilities of OH ($X^2\Pi$), J. Mol. Spectrosc., 53, 150–188, 1974.

Molina, A., Lopez-Puertas, M., Lopez-Moreno, J. J., and Rodrigo, R.: Gravity waves from five simultaneous emissions – OH (6-2), NaD, O_2 ($^1\Sigma$), O I-557.7 nm, and the visible continuum, Can. J. Phys., 63, 592–599, 1985.

Mukhtarov, Pl., Andonov, B., Borries, C., Pancheva, D., and Jakowski, N.: Forcing of the ionosphere from above and below during the Arctic winter of 2005/2006, J. Atmos. Solar-Terr. Phys., 72, 193–205, doi:10.1016/j.jastp.2009.11.008, 2010.

Pancheva, D., Mitchell, N. J., and Younger, P. T.: Meteor radar observations of atmospheric waves in the equatorial mesosphere/lower thermosphere over Ascension Island, Ann. Geophys., 22, 387–404, doi:10.5194/angeo-22-387-2004, 2004.

Pancheva, D., Mukhtarov, P., and Andonov, B.: Global structure, seasonal and interannual variability of the migrating semidiurnal tide seen in the SABER/TIMED temperatures (2002–2007), Ann. Geophys., 27, 687–703, doi:10.5194/angeo-27-687-2009, 2009a.

Pancheva, D., Mukhtarov, P., Andonov, B., Mitchell, N. J., and Forbes, J. M.: Planetary waves observed by TIMED/SABER in coupling the stratosphere-mesosphere-lower thermosphere during the winter of 2003/2004: Part 2 – Altitude and latitude planetary wave structure, J. Atmos. Solar-Terr. Phys., 71, 75–87, doi:10.1016/j.jastp.2008.09.027, 2009b.

Parihar, N. and Mukherjee, G. K.: Measurement of mesopause temperature from hydroxyl nightglow at Kolhapur (16.8° N, 74.2° E), India, Adv. Space Res., 41, 660–669, doi:10.1016/j.asr.2007.05.002, 2008.

Parihar, N., Gurubaran, S., and Mukherjee, G. K.: Observations of OI 557.7 nm nightglow at Kolhapur (17° N), India, Ann. Geophys., 29, 1873–1884, doi:10.5194/angeo-29-1873-2011, 2011.

Petitdidier, M. and Teitelbaum, H.: Lower thermosphere emissions and tides, Planet. Space Sci., 25, 711–721, 1977.

Scheer, J.: Programmable tilting filter spectrometer for studying gravity waves in the upper atmosphere, Appl. Optics, 26, 3077–3082, 1987.

Scheer, J. and Reisin, E. R.: Rotational temperatures for OH and O_2 airglow bands measured simultaneously from El Leoncito (31°48′ S), J. Atmos. Terr. Phys., 52, 47–57, 1990.

She, C. Y. and Lowe, R. P.: Seasonal temperature variations in the mesopause region at mid-latitude: comparison of lidar and hydroxyl rotational temperatures using WINDII/ UARS OH height profiles, J. Atmos. Solar-Terr. Phys., 60, 1573–1583, 1998.

Shepherd, M. and Fricke-Begemann, C.: Study of the tidal variations in mesospheric temperature at low and mid latitudes from WINDII and potassium lidar observations, Ann. Geophys., 22, 1513–1528, doi:10.5194/angeo-22-1513-2004, 2004.

Sivjee, G. G. and Hamwey, R. M.: Temperature and chemistry of the polar mesopause OH, J. Geophys. Res., 92, 4663–4672, 1987.

Smith, A. K.: Physics and chemistry of the mesopause region, J. Atmos. Solar-Terr. Phys., 66, 839–857, doi:10.1016/j.jastp.2004.01.032, 2004.

Sridharan, R., Taori, A., Gurubaran, S., Rajaram, R., and Shepherd, M. G.: First results on daytime mesopause OH rotational temperatures using ground-based photometry from equatorial latitudes, J. Atmos. Solar-Terr. Phys., 61, 1131–1142, doi:10.1016/S1364-6826(99)00062-0, 1999.

Sridharan, S., Gurubaran, S., and Rajaram, R.: Radar observations of the 3.5-day ultra-fast Kelvin wave in the low-latitude mesopause region, J. Atmos. Solar-Terr. Phys., 64, 1241–1250, 2002.

Takahashi, H., Batista, P. P., Clemesha, B. R., Simonich, D. M., and Sahai, Y.: Correlations between OH, NaD, and OI 5577 Å emissions in the airglow, Planet. Space Sci., 27, 801–807, 1979.

Takahashi, H., Sahai, Y., and Batista, P. P.: Airglow $O_2(^1\Sigma)$ atmospheric band at 8645 Å and the rotational temperature observed at 23° S, Planet. Space Sci., 34, 301–306, 1986.

Takahashi, H., Melo, S. M. L., Clemesha, B. R., Simonich, D. M., Stegman, J., and Witt, G.: Atomic hydrogen and ozone concentrations derived from simultaneous lidar and rocket airglow measurements in the equatorial region, J. Geophys. Res., 101, 4033–4040, 1996.

Takahashi, H., Gobbi, D., Batista, P. P., Melo, S. M. L., Teixeira, N. R., and Buriti, R. A.: Dynamical influence on the equatorial airglow observed from the south american sector, Adv. Space Res., 21, 817–825, 1998.

Takahashi, H., Buriti, R. A., Gobbi, D., and Batista, P. P.: Equatorial planetary wave signatures observed in mesospheric airglow emissions, J. Atmos. Solar-Terr. Phys., 64, 1263–1272, 2002.

Taori, A. and Taylor, M. J.: Dominant winter-time mesospheric wave signatures over a low latitude station, Hawaii (20.8° N): An investigation, J. Earth Syst. Sci., 119, 259–264, 2010.

Taori, A., Kalamakar, V., Raghunath, K., Rao, S. V. B., and Russell III, J. M.: Simultaneous Rayleigh lidar and airglow measurements of middle atmospheric waves over low latitudes in India, J. Atmos. Solar-Terr. Phys., 78–79, 62–69, doi:10.1016/j.jastp.2011.06.012, 2012a.

Taori, A., Kamalakar, V., and Jayaraman, A.: First observation of upper mesospheric semi annual oscillations using ground based airglow measurements from Indian low latitudes, Adv. Space Res., 49, 937–942, doi:10.1016/j.asr.2011.12.016, 2012b.

Taori, A., Kesarkar, A. P., Niranjan Kumar, K., and Ramkumar, T. K.: A case of sudden variation in nocturnal mesospheric temperatures: Variabilitiy and its causative mechanism, J. Atmos. Solar-Terr. Phys., 78–79, 125–131, doi:10.1016/j.jastp.2011.04.020, 2012c.

Ward, W. E.: Tidal mechanisms of dynamical influence on oxygen recombination reaction airglow in the mesosphere and lower thermosphere, Adv. Space Res., 21, 795–805, 1998.

Xu, J., Liu, H.-L., Yuan, W., Smith, A. K., Roble, R. G., Mertens, C. J., Russell III, J. M., and Mlynczak, M. G.: Mesopause structure from Thermosphere, Ionosphere, Mesosphere, Energetics, and Dynamics (TIMED)/Sounding of the Atmosphere Using Broadband Emission Radiometry (SABER) observations, J. Geophys. Res., 112, D09102, doi:10.1029/2006JD007711, 2007.

Yee, J. -H., Crowley, G., Roble, R. G., Skinner, W. R., Burrage, M. D., and Hays, P. B.: Global simulations and observations of O (^{1}S), O_2 ($^1\Sigma$) and OH mesospheric nightglow emissions, J. Geophys. Res., 102, 19949–19968, 1997.

Zhang, S. P. and Shepherd, G. G.: The influence of the diurnal tide on the O (^{1}S) and OH emission rates observed by WINDII on UARS, Geophys. Res. Lett., 26, 529–532, 1999.

Zhang, X., Forbes, J. M., Hagan, M. E., Russell III, J. M., Palo, S. E., Mertens, C. J., and Mlynczak, M. G.: Monthly tidal temperatures 20–120 km from TIMED/SABER, J. Geophys. Res., 111, A10S08, doi:10.1029/2005JA011504, 2006.